
Pseudo-Invertible Neural Networks

Yamit Ehrlich¹ Nimrod Berman² Assaf Shocher¹

Abstract

The Moore-Penrose Pseudo-inverse (PInv) serves as the fundamental solution for linear systems. In this paper, we propose a natural generalization of PInv to the nonlinear regime in general and to neural networks in particular. We introduce **Surjective Pseudo-invertible Neural Networks (SPNN)**, a class of architectures explicitly designed to admit a tractable non-linear PInv. The proposed non-linear PInv and its implementation in SPNN satisfy fundamental geometric properties. One such property is null-space projection or "Back-Projection", $x' = x + A^\dagger(y - Ax)$, which moves a sample x to its closest consistent state x' satisfying $Ax = y$. We formalize **Non-Linear Back-Projection (NLBP)**, a method that guarantees the same consistency constraint for non-linear mappings $f(x) = y$ via our defined PInv. We leverage SPNNs to expand the scope of zero-shot inverse problems. Diffusion-based null-space projection has revolutionized zero-shot solving for linear inverse problems by exploiting closed-form back-projection. We extend this method to non-linear degradations. Here, "degradation" is broadly generalized to include any non-linear loss of information, spanning from optical distortions to semantic abstractions like classification. This approach enables zero-shot inversion of complex degradations and allows precise semantic control over generative outputs without retraining the diffusion prior.

1. Introduction

The concept of a generalized inverse is foundational to signal processing and data analysis. In the linear regime, the Moore-Penrose pseudo-inverse (PInv) serves as the canonical solution, providing a rigorous framework for inverting singular operators. While typically computed via SVD, it is formally defined by the four Penrose Identities (Penrose,

¹Technion ²Ben-Gurion University. Correspondence to: Yamit Ehrlich <yamitehrlich@campus.technion.ac.il >.

1955). Uniquely, the PInv guarantees the **minimal-norm solution** among all valid inverses, while simultaneously providing the **optimal least-squares (MMSE) approximation** when no exact solution exists. Furthermore, it enables exact consistency enforcement via null-space back-projection, allowing one to project any vector onto its closest consistent state. These properties make the PInv indispensable for diverse applications.

In contrast, "inversion" in modern Deep Learning is typically approached either as a regression task (autoencoders) or a probabilistic generation task (conditional diffusion). While empirically effective, these approaches lack the structural guarantees of their linear counterparts, failing to satisfy reflexive consistency ($f(f^{-1}(f(x))) \neq f(x)$). Conversely, architectures that do enforce rigorous invertibility, such as Invertible Neural Networks (INNs) and Normalizing Flows, are constrained by strict bijectivity. To ensure tractability, they must preserve dimensionality, rendering them unsuitable for tasks where information is discarded, such as classification and many others.

In this work, we propose a natural generalization of the PInv to the non-linear regime. We define this operator by strictly maintaining the first two Penrose identities ($gg^\dagger g = g$ and $g^\dagger gg^\dagger = g^\dagger$), ensuring reflexive consistency between the forward and inverse mappings. This aligns with (Gofer & Gilboa, 2023). The final two Penrose identities, however, are inapplicable in the non-linear setting as they rely on the linear adjoint. This leaves a challenge of choosing the unique PInv out of the set of generalized inverses. Differently from Gofer & Gilboa, who define the PInv as the one that minimizes the norm $\|g^\dagger(y)\|$, we propose a different definition: we define the PInv as the unique solution induced by a Bijective Completion of the operator. While both approaches are equivalent in the linear regime, they diverge in the non-linear case. We show in § 4 that this definition makes the most natural choice for PInv.

We introduce **Surjective Pseudo-invertible Neural Networks (SPNN)**, a class of architectures designed to model surjective mappings where the input dimensionality exceeds the output, resulting in explicit information loss. Unlike standard networks, SPNNs possess a **built-in Pseudo-Inverse** by construction. This is achieved via a surjective coupling mechanism, where the residual degrees of freedom are resolved by a learned auxiliary network. This auxiliary

component is optimized to resolve the ambiguity by selecting the unique solution that minimizes the induced norm, effectively implementing our proposed non-linear PInv.

This algebraic framework unlocks powerful applications for zero-shot restoration and analysis. We leverage SPNNs to introduce Non-Linear Back-Projection (NLBP), which projects inputs onto the pre-image of non-linear surjective mappings. As a demonstration of the framework’s capabilities, we show how NLBP enables precise semantic control over generative outputs without retraining.

Our main contributions are summarized as follows:

- **Non-linear Pseudo-inverse:** We propose a natural definition for the non-linear pseudo-inverse justified by coordinate consistency and consistent properties.
- **SPNN:** We introduce the first deep architecture to admit a tractable, unique PInv that satisfies this definition and the Penrose identities by construction.
- **Non-Linear Back-Projection (NLBP):** We generalize Iterative Back-Projection to the non-linear regime, enabling zero-shot solution of complex inverse problems.

2. Related Work

Deep Invertible Architectures. The structural foundation of modern invertible networks traces back to the 1970s in cryptography with the Feistel Cipher (Feistel, 1973), which introduced the concept of splitting data into halves and modifying one half conditioned on the other to ensure exact reversibility. In deep learning, this structure was revitalized by NICE (Non-linear Independent Components Estimation) (Dinh et al., 2014), which proposed additive coupling layers to enforce a tractable Jacobian determinant of unity. This was subsequently improved by RealNVP (Dinh et al., 2017), which utilized affine coupling layers (incorporating scaling) to enhance expressivity, and Glow (Kingma & Dhariwal, 2018), which introduced invertible 1x1 convolutions to replace fixed channel permutations with learnable unitary mixing, often parameterized via Cayley transforms (Trockman & Kolter, 2021).

Surjective Architectures. While standard flows are restricted to bijectivity, SurVAE Flows (Nielsen et al., 2020) introduced a framework of surjective layers (e.g., pooling, slicing) to bridge the gap between VAEs and Flows. Our SPNN architecture shares the structural use of surjective coupling blocks where input dimensions are split and partially discarded. However, we diverge fundamentally in objective: whereas SurVAE optimizes a stochastic lower bound on the likelihood (ELBO) (Nielsen et al., 2020), SPNNs utilize a deterministic auxiliary network to explicitly model the unique PInv. This transforms the architecture from a

probabilistic generative model into an algebraic operator that learns the unique *non-linear PInv*.

Generalized Inversion of Non-Linear Operators. The theory of generalized inverses is well-established for linear operators, with the Moore-Penrose inverse serving as the canonical solution satisfying the algebraic Penrose identities. Recently, Gofer and Gilboa (Gofer & Gilboa, 2023) established a theoretical framework for non-linear pseudo-inversion, proposing that the unique “pseudo-inverse” in metric spaces be defined by the *Best Approximate Solution (BAS)* property, replacing the linear adjoint condition with a minimal-norm constraint on the pre-image.

Zero-Shot Inverse Problems. Pretrained diffusion models have emerged as state-of-the-art priors for solving inverse problems $y = \mathcal{D}(x)$ zero-shot. Current methods generally follow two paradigms:

Null-Space Methods (Linear): Approaches like DDRM (Kawar et al., 2022), DDNM (Wang et al., 2023), and SNIPS (Kawar et al., 2021) exploit the SVD of the degradation matrix to project diffusion samples onto the measurement subspace ($x' = x + A^\dagger(y - Ax)$). These provide stable, closed-form consistency but are strictly limited to linear degradations.

Gradient Guidance (Non-Linear): Methods like DPS (Diffusion Posterior Sampling) (Chung et al., 2023) and PnP-Diffusion (Chung et al., 2022) handle non-linear operators by backpropagating the error $\nabla_x \|y - \mathcal{D}(x)\|^2$ through the network. This requires differentiable forward models and often suffers from gradient instability during the noisy stages of generation.

Our Non-Linear Back-Projection (NLBP) unifies these approaches by generalizing the classic *Iterative Back-Projection (IBP)* algorithm of Irani and Peleg (Irani & Peleg, 1991) to the deep learning era. By replacing the heuristic kernel of IBP with a learned, structural PInv \mathcal{D}^\dagger , we achieve the stability of null-space projection for arbitrary non-linear degradations.

3. Preliminaries

3.1. Basic Notions of Invertibility

The invertibility of an operator $g : \mathcal{X} \rightarrow \mathcal{Y}$ is strictly determined by its mapping characteristics. If g is **injective** (one-to-one), it preserves distinctness, guaranteeing that no information is lost during the mapping. This allows for a **Left Inverse** $g_L^{-1} : \mathcal{Y} \rightarrow \mathcal{X}$ satisfying:

$$g_L^{-1} \circ g = \text{Id}_{\mathcal{X}}, \tag{1}$$

which perfectly recovers the input x .

Conversely, if g is **surjective** (onto), its range covers the entire target space \mathcal{Y} . This guarantees that every target y is reachable, allowing for a **Right Inverse** $g_R^{-1} : \mathcal{Y} \rightarrow \mathcal{X}$

satisfying:

$$g \circ g_R^{-1} = \text{Id}_{\mathcal{Y}}. \quad (2)$$

When an operator is both injective and surjective (bijective), it admits a unique two-sided **Inverse** g^{-1} .

3.2. The Linear Moore-Penrose Standard

For a linear operator $A \in \mathbb{C}^{m \times n}$, the Moore-Penrose PInv $A^\dagger \in \mathbb{C}^{n \times m}$ is the unique matrix satisfying the four Penrose identities:

$$AA^\dagger A = A, \quad (3)$$

$$A^\dagger AA^\dagger = A^\dagger, \quad (4)$$

$$(AA^\dagger)^* = AA^\dagger, \quad (5)$$

$$(A^\dagger A)^* = A^\dagger A. \quad (6)$$

Equations (3) and (4) establish *reflexive consistency*, ensuring that A^\dagger acts as a generalized inverse. Equations (5) and (6) enforce that the projection operators AA^\dagger and $A^\dagger A$ are orthogonal (Hermitian), which is crucial for the least-squares and minimal-norm properties of the solution. Specifically, for any y , $x^* = A^\dagger y$ is the unique vector that minimizes $\|x\|_2$ among all minimizers of $\|Ax - y\|_2$.

3.3. Back-Projection

A fundamental property derived from these identities is the capacity to project an arbitrary vector onto the solution space. Given an initial estimate x and a measurement y , the update:

$$x' = x + A^\dagger(y - Ax) \quad (7)$$

yields the unique vector x' that is closest to x (in the Euclidean norm $\|x' - x\|_2$) subject to the consistency constraint $Ax' = y$ (assuming y lies in the range of A). This property is the cornerstone of null-space methods for inverse problems, allowing one to enforce measurement fidelity without destroying the prior information contained in x .

3.4. Generalized Non-Linear Inversion

Extending this concept to a non-linear operator $g : \mathcal{X} \rightarrow \mathcal{Y}$ is non-trivial, as the adjoint operator (required for Eqs. (5)-(6)) is not generally defined. However, the first two Penrose identities ($gg^\dagger g = g$ and $g^\dagger gg^\dagger = g^\dagger$) rely solely on composition and can be applied to any mapping.

Satisfying these two identities guarantees *Reflexive Consistency*, but it does not yield a unique solution. To resolve this ambiguity, (Gofer & Gilboa, 2023) proposed adopting the variational principle of the linear PInv. They define the unique non-linear pseudo-inverse as the specific right-inverse that recovers the **minimal-norm** element of the pre-image ($\text{argmin}_{x \in g^{-1}(y)} \|x\|$). This effectively generalizes the linear "closest solution to zero" property to the non-linear regime.

3.5. Iterative Back-Projection (IBP)

While Eq. (7) provides a one-step projection for ideal linear cases, many inverse problems such as Super-Resolution (SR) require iterative refinement to handle ill-posedness and accumulate details. Irani and Peleg (Irani & Peleg, 1991) formalized this with the Iterative Back-Projection (IBP) algorithm.

Designed originally for SR, IBP minimizes the reconstruction error by iteratively adding the "back-projected" error to the estimate:

$$x_{k+1} = x_k + \lambda H(y - Ax_k), \quad (8)$$

where H is a back-projection kernel (approximating A^\dagger) and λ is a step size. This process essentially applies the logic of Eq. (7) repeatedly, steering the candidate image x_k towards measurement consistency while relying on the starting point x_0 as a prior.

4. Non-Linear Pseudo-Inverse

In the linear regime, the Moore-Penrose Pseudo-Inverse is canonically defined as the unique operator satisfying the four Penrose identities. Extending this to the non-linear setting presents a challenge: the final two Penrose identities rely on the linear adjoint and are thus inapplicable. To resolve this ambiguity, we propose a definition that is the natural generalization. We base it on bijective completion and provide justifications for the naturality of this definition.

Definition 4.1 (Bijective Completion). Let $g : \mathcal{X} \rightarrow \mathcal{Y}$ be a surjective continuous operator. A **Bijective Completion** is a diffeomorphism $G : \mathcal{X} \rightarrow \mathcal{Y} \times \mathcal{Z}$ defined as:

$$G(x) = [g(x)|q(x)]^T \quad (9)$$

where $q : \mathcal{X} \rightarrow \mathcal{Z}$ is surjective

Definition 4.2 (The Natural Non-Linear PInv). Given a surjective operator g and a fixed Bijective Completion G , the **Natural Non-Linear Pseudo-Inverse induced by G** , denoted g^\dagger , is the operator that selects the unique solution in the pre-image minimizing the distance to the origin in the completed space:

$$g^\dagger(y) = \text{argmin}_{x \in g^{-1}(y)} \|G(x) - G(0)\|_2. \quad (10)$$

4.1. Theoretical Justification

We justify this definition by demonstrating that it preserves three fundamental properties that characterize the linear pseudo-inverse.

1. Reflexive Consistency. Our definition satisfies the reflexive Penrose identities ($gg^\dagger g = g$ and $g^\dagger gg^\dagger = g^\dagger$) by construction. The first identity follows directly from the pre-image constraint ($g(g^\dagger(y)) = y$). The second follows

from the uniqueness of the minimizer: since g^\dagger maps to a unique section of the manifold (where $\|G(x) - G(0)\|$ is minimized), applying g and then g^\dagger consistently returns to this same section. This part also aligns with (Gofer & Gilboa, 2023).

2. Coordinate Consistency. If g 's non-linearity is purely coordinate transformation, the correct inverse should respect the underlying linear structure. Consider $g(x) = A\phi(x)$ where ϕ is a diffeomorphism with $\phi(0) = 0$ and A is linear surjective. Since A is linear in the ϕ -coordinates, the Moore-Penrose inverse A^\dagger gives the canonical solution there, yielding $g^\dagger(y) = \phi^{-1}(A^\dagger y)$. Minimizing $\|x\|$ over the pre-image (as in Gofer & Gilboa) ignores this geometric structure and produces an incorrect solution. Our definition recovers the correct inverse: the natural completion is $G(x) = \phi(x)$ (including null-space components), so minimizing $\|G(x) - G(0)\| = \|\phi(x)\|$ yields $\phi^{-1}(A^\dagger y)$ as required.

3. Back-Projection Consistency. Eq. 7 provides a closed form for finding the closest vector that satisfies a linear constraint. A non-linear PInv is expected to be used in an equivalent non-linear closed form. We propose an equivalent Non-Linear Back-Projection (NLBP). We demonstrate that this formulation is robust: it guarantees convergence to the valid pre-image for *any* reflexive generalized inverse. However, we further show that for this update to act as an *orthogonal projection*, specifically finding the closest solution to the initial estimate, the pseudo-inverse must strictly adhere to our proposed definition in Eq. 10.

Definition 4.3 (Non-Linear Back-Projection). Let g be a surjective continuous function and G a bijective completion of it. We define the Non-Linear Back-Projection (NLBP) x' w.r.t. G given x, y as follows:

$$x' = G^{-1}(G(x) - G(g^\dagger(g(x))) + G(g^\dagger(y))). \quad (11)$$

Claim 1. For any g^\dagger that satisfies the reflexive Penrose identities (3),(4), x' is on the pre-image of y , satisfying $g(x') = y$.

Proof. By definition, $G(x)$ decomposes into $[g(x)|q(x)]^T$. The range component of the update in Eq. (11) is:

$$g(x') = g(x) - g(g^\dagger(g(x))) + g(g^\dagger(y)). \quad (12)$$

The second of the three terms in the right hand side, reduces to $g(x)$ according to First Penrose identity (3). The third reduces to y due to g being surjective. Thus:

$$g(x') = g(x) - g(x) + y = y. \quad (13)$$

□

Claim 2. The update x' is the orthogonal projection of x onto the solution manifold $g^{-1}(y)$ in the G -metric.

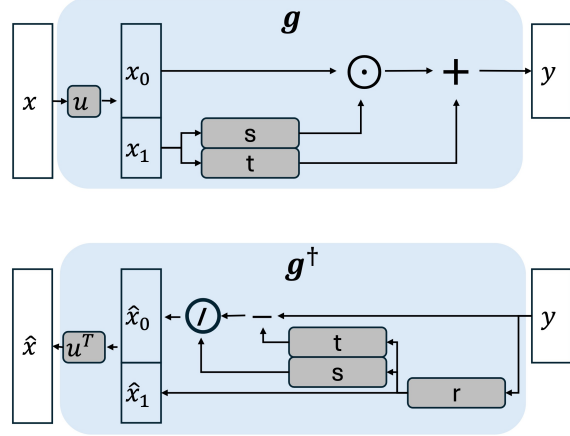


Figure 1. The SPNN Block Architecture. Top (Forward g): The input x is rotated by u and split. The null-space component x_1 modulates the signal x_0 via affine coupling layers (s, t) to produce the compressed output y . **Bottom (Pseudo-Inverse g^\dagger):** An auxiliary network r predicts the missing null-space information \hat{x}_1 solely from y , allowing the reverse coupling flow to structurally reconstruct the high-dimensional pre-image \hat{x} .

Proof. Let $\Delta x = x' - x$. We analyze the components of this displacement in the latent space of G . The range component is fixed by the target: $g(x') - g(x) = y - g(x)$. The null-space component is derived from Eq. (11):

$$q(x') - q(x) = q(g^\dagger(y)) - q(g^\dagger(g(x))). \quad (14)$$

By Definition 4.2, $g^\dagger(\cdot)$ always selects the unique minimizer $q(z) = q(0)$. Thus, both terms on the RHS are identical constants ($q(0)$), and they cancel out:

$$q(x') - q(x) = 0. \quad (15)$$

The latent displacement vector is therefore $\Delta G = [y - g(x)|0]^T$. Any tangent vector v to the solution manifold (where $g(z) = y$ is constant) must have the form $dG(v) = [0, dq]^T$. The inner product is zero:

$$\langle \Delta G, dG(v) \rangle = (y - g(x))^T \cdot 0 + 0^T \cdot dq = 0. \quad \square \quad (16)$$

5. Surjective Pseudo-invertible Neural Network (SPNN)

In this section, we introduce the Surjective Pseudo-invertible Neural Network (SPNN). Unlike standard Invertible Neural Networks (INNs) that preserve dimensionality to ensure bijectivity, SPNNs are designed to be dimension-reducing ($d \leq D$) while maintaining a rigorous, structural inverse.

5.1. Surjective Pseudo-Invertible Block

The fundamental building block of our architecture is the Affine Surjective Coupling Block. Let $x \in \mathbb{R}^D$ be the input to a layer. We first partition the input into two vectors:

$$x \rightarrow [x_0 | x_1], \quad \text{where } x_0 \in \mathbb{R}^d, \quad x_1 \in \mathbb{R}^{D-d}. \quad (17)$$

The forward operation $g(\cdot)$ is defined as an **affine coupling**, where x_1 modulates x_0 via learned scale and translation functions:

$$y = x_0 \odot s(x_1) + t(x_1), \quad (18)$$

where $s, t : \mathbb{R}^{D-d} \rightarrow \mathbb{R}^d$ are arbitrary non-linear neural networks (e.g., MLPs or CNNs), and \odot denotes element-wise multiplication. The output $y \in \mathbb{R}^d$ has strictly lower dimensionality than the input, making the operation inherently surjective.

To define the PInv $g^\dagger(y)$, we must resolve the unknown components x_1 . We introduce a learnable auxiliary network $r : \mathbb{R}^d \rightarrow \mathbb{R}^{D-d}$ responsible for predicting the discarded vector from the compressed code y . The inverse operation proceeds in two steps (see Figure 1):

$$\hat{x}_1 = r(y), \quad (19)$$

$$\hat{x}_0 = \frac{y - t(\hat{x}_1)}{s(\hat{x}_1)}. \quad (20)$$

The reconstructed input is then formed by concatenating: $\hat{x} = [\hat{x}_0 \mid \hat{x}_1]$.

5.2. Two-Phase Training Strategy

The training of an SPNN decomposes naturally into two distinct phases. This separation allows us to optimize the forward performance without compromise, and subsequently learn the optimal inverse manifold.

Phase I: Task Learning. First, we optimize the parameters of the forward operation ($\theta_g = \{s, t, U\}$) to approximate the target function. Depending on the problem, we minimize a task-specific objective \mathcal{L}_{task} (e.g., Cross-Entropy for classification or MSE for compression). Crucially, because the auxiliary network r is not involved in the forward pass (except for regularization), this phase is identical to training a standard feed-forward network or flow model. Once converged, the forward parameters θ_g are frozen.

Phase II: Natural Inverse Learning. In the second phase, we optimize the auxiliary network r to satisfy the geometric requirements of the **Natural Non-Linear Pseudo-Inverse**. While the architecture guarantees the Penrose identities by construction, r provides the degree of freedom necessary to select the specific solution that satisfies the minimality constraint.

We optimize r to minimize the deviation of the solution from the geometric center of the bijective completion G :

$$\mathcal{L}_{natural} = \mathbb{E}_y [\|G(g^\dagger(y)) - G(0)\|_2^2]. \quad (21)$$

By minimizing this loss, r learns to predict the specific missing components (\hat{x}_1) that place the solution on the principal section of the manifold. This effectively forces g^\dagger to become the unique Natural PInv (Definition 4.2) rather than an arbitrary generalized inverse.

5.3. Theoretical Analysis

We now prove that this specific affine construction satisfies the rigorous algebraic requirements of a generalized inverse.

Theorem 5.1 (Surjectivity / Exact Right-Inverse). *The operator g^\dagger defined in Eqs. (19)-(20) is a strict right-inverse of g , satisfying $g(g^\dagger(y)) = y$ for all $y \in \mathbb{R}^d$.*

Proof. Let y be an arbitrary vector. Applying the pseudo-inverse yields $\hat{x}_1 = r(y)$ and $\hat{x}_0 = (y - t(\hat{x}_1)) \odot s(\hat{x}_1)$. Substituting these back into the forward operator g :

$$\begin{aligned} g(\hat{x}) &= \hat{x}_0 \odot s(\hat{x}_1) + t(\hat{x}_1) \\ &= \left(\frac{y - t(r(y))}{s(r(y))} \right) \odot s(r(y)) + t(r(y)) \\ &= (y - t(r(y))) + t(r(y)) \\ &= y. \end{aligned}$$

Thus, $gg^\dagger = I$, confirming surjectivity. \square

Theorem 5.2 (Reflexive Consistency). *The SPNN architecture satisfies the first two Penrose identities by construction, regardless of the choice of networks s, t, r .*

Proof. **Identity 1** ($gg^\dagger g = g$): Since $gg^\dagger = I$ (Theorem 1), we have $(gg^\dagger)g = I \cdot g = g$.

Identity 2 ($g^\dagger gg^\dagger = g^\dagger$): Similarly, substituting the identity into the right side: $g^\dagger(gg^\dagger) = g^\dagger \cdot I = g^\dagger$. \square

5.4. Implementation Details

Multi-Scale Architecture. The SPNN is constructed as a deep sequence of reversible blocks. To process high-dimensional image data effectively, we employ a multi-scale architecture. We utilize the `PixelUnshuffle` operation to trade spatial resolution for channel depth, effectively reducing the spatial dimensions while quadrupling the number of channels. This downsampled representation is then processed by one or more SPNN blocks. Each block splits the channel dimensions, passing a subset of "informative" channels (x_0) to the next stage while discarding the "redundant" channels (x_1) via the forward operation. This hierarchical reduction allows the network to capture semantic features at varying scales while progressively reducing the dimensionality towards the target size d .

Orthogonal Mixing. Standard coupling layers operate on fixed channel splits (e.g., splitting the first k channels). However, adjacent channels in image data (like RGB) are often highly correlated, and a naive split may restrict the expressivity of the null-space. To address this, we precede each split operation with a learnable unitary matrix U , parameterized via the Cayley transform to ensure exact orthogonality ($U^\top U = I$) by construction. This learnable rotation allows

the network to discover the optimal basis for separating the signal into "content" (x_0) and "redundancy" (x_1) before the information is discarded.

Auxiliary Stability Losses. While the SPNN architecture structurally guarantees the inverse properties, finite-precision arithmetic can lead to numerical drift. To mitigate this, we employ two auxiliary losses throughout the training phases. First, we apply a *Surjectivity Consistency* loss: $\|y - g(g^\dagger(y))\|_2^2$. Although theoretically zero by construction, minimizing this term explicitly combats floating-point error accumulation during deep inverse passes. Second, we apply a *Pseudo-Inverse Stability* loss: $\|x - g^\dagger(g(x))\|_2^2$. Since $d < D$, exact reconstruction is impossible; however, minimizing this expectation encourages the pseudo-inverse to map outputs back to the typical range of the data distribution. This acts as a regularizer, preventing the inverse path from generating extreme numerical values that could destabilize the training dynamics.

6. Iterative Restoration via Non-Linear Back-Projection

The properties of the SPNN and NLBP open a new avenue for solving non-linear inverse problems. While standard methods focus on linear corruptions (blur, inpainting), many real-world "degradations" are inherently non-linear. These range from complex hardware distortions (ISP pipelines, JPEG compression) to semantic abstractions, where the "degradation" is a classifier or a captioning network effectively reducing an image to a label or a string. SPNNs allow us to expose the null-space structure of such operators for controlled restoration.

6.1. Modeling Degradations

We treat the degradation process as a black box $\mathcal{D}(x)$. We train an SPNN g to approximate this operator ($g(x) \approx \mathcal{D}(x)$) using the training methodology described in Section 5.

6.2. Zero-Shot Restoration with Diffusion

We propose an iterative restoration algorithm inspired by linear methods like DDNM (Wang et al., 2022), utilizing our **Natural Non-Linear Back-Projection (NLBP)** to guide the generation.

We integrate the NLBP into a pre-trained diffusion sampling loop. At each timestep t , given a clean estimate $\hat{x}_{0|t}$ and a target observation y , we apply a "gentle" version of our projection to enforce consistency. The update rule is defined as:

$$\hat{x}'_{0|t} = G^{-1} \left(G(\hat{x}_{0|t}) + \lambda [G(g^\dagger(y)) - G(g^\dagger(g(\hat{x}_{0|t})))] \right), \quad (22)$$

where $\lambda \in [0, 1]$ is a guidance scale.

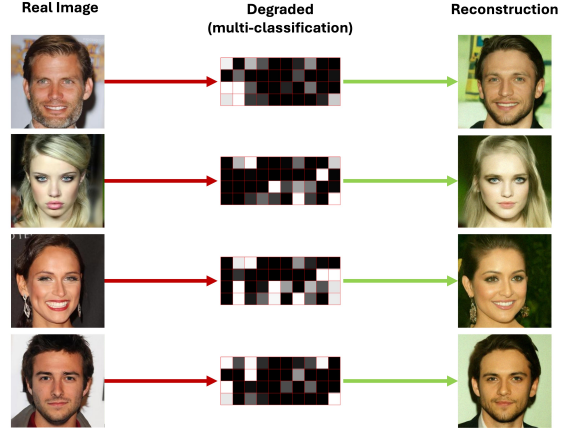


Figure 2. **Reconstruction from Semantics.** We project a clean image (Left) into its 40-dimensional attribute vector (as a row-major grid, middle), see Appendix A or fig. 3 for a list of attributes. Using only this low-dimensional semantic code, our NLBP guides the diffusion model to reconstruct a photorealistic face (Right) that faithfully preserves the attributes of the original subject.

Substituting the latent decomposition of the difference term ($[y - g(\hat{x}_{0|t}) \mid 0]^T$) reveals the mechanics of this update:

$$g(\hat{x}'_{0|t}) = (1 - \lambda)g(\hat{x}_{0|t}) + \lambda y, \quad (23)$$

$$q(\hat{x}'_{0|t}) = q(\hat{x}_{0|t}). \quad (24)$$

This formulation allows us to steer the semantic content (range) towards the observation y via linear interpolation, while the high-frequency details (null-space) generated by the diffusion prior remain strictly invariant ($q_{new} = q_{old}$). This enables the reconstruction of consistent images from highly compressed inputs, such as class labels or thumbnails, without disrupting the texture coherence of the generative model.

Algorithm 1 Non-Linear Null-Space Projection (Simplification)

Input: Measurement y , Diffusion Model ϵ_θ , SPNN G , Scale λ

Initialize $x_T \sim \mathcal{N}(0, I)$

for $t = T, \dots, 1$ **do**

$\hat{x}_{0|t} \leftarrow$ Predict x_0 from x_t using $\epsilon_\theta(x_t, t)$

$\hat{x}'_{0|t} \leftarrow$ NLBP($\hat{x}_{0|t}, y, \lambda$) {Eq. 22}

$x_{t-1} \leftarrow$ Sample $q(x_{t-1} | \hat{x}'_{0|t}, x_t)$

end for

Return x_0

7. NLBP Implementation Details

We implement the Non-Linear Back-Projection (NLBP) within a standard diffusion sampling framework, adopting the structure of DDNM (Wang et al., 2022).

Diffusion Backbone. We utilize a pre-trained unconditional DDPM with $T = 1000$ timesteps. The reverse diffusion process follows the standard noise schedule β_t . At each timestep t , we estimate $\hat{x}_{0|t}$ via the denoising network and apply the NLBP correction before re-sampling x_{t-1} .

Reconstruction Strategy. We do not start applying NLBP from the first sampling step. We find that in early steps, the predicted images is too blurry and noisy and is out of distribution for the degradation network, so we wait for the generated image to be closer to distribution. Out of the 1000 steps (going $1000 \rightarrow 0$) we start at step 800 for the semantic reconstruction task and from 500 for the attribute-controlled generation task.

Adaptive Lambda. For single-attribute editing (Figure 4) and multi-attribute editing (Figure 5), we scale λ dynamically based on the discrepancy between the current state and the target. Let $\delta_n = |y_{cur}[n] - y_{target}[n]|$ be the distance for the controlled attribute n . We set $\lambda_t = \alpha \cdot \tanh(\gamma \cdot \delta_n)$, ensuring stronger guidance when the attribute is far from the target and gentler updates as it converges.

8. Experiments

We evaluate the proposed framework on a challenging class of non-linear inverse problems: **Semantic Restoration**. In this setting, the forward operator is a semantic abstraction (classification), meaning the "measurement" contains no spatial information, only high-level descriptors.

8.1. Data and Setup

We utilize the CelebA-HQ dataset, downsampled to 256×256 resolution. The dataset contains facial images annotated with 40 binary attributes (e.g., *Male*, *Smiling*, *Eyeglasses*). **Forward Operator (g).** We define the non-linear operator as the mapping from pixel space to the 40-dimensional attribute logit space. We train an SPNN (g_θ) directly on the image-attribute pairs to approximate this function.

Generative Prior. We employ a standard unconditional DDPM trained on the same 256×256 CelebA-HQ images to serve as the generative prior.

8.2. Results

Reconstruction from Semantics. We aim to reconstruct a face given *only* its semantic classification. We first extract the ground-truth logits $y_{GT} = g(x_{orig})$ from an unseen test image. We then perform the diffusion sampling process guided by NLBP (Eq. 22) with y_{GT} as the fixed target. Fig 2 visualizes the results. The method successfully hallucinates a valid pre-image that matches the semantic constraints while filling in the null-space with plausible details.

To quantify this fidelity, we computed the reconstruction ac-

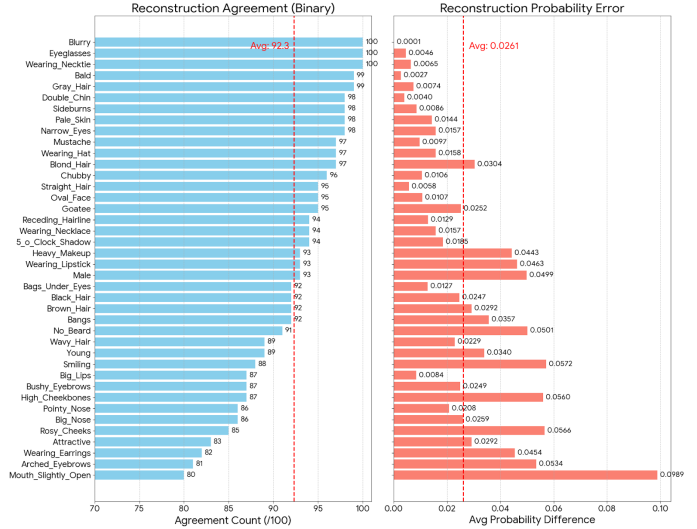


Figure 3. **Quantitative Attribute Reconstruction.** Analysis of 100 test samples. **Left:** Binary agreement rate. **Right:** Mean absolute error in probability space.

curacy over 100 randomly selected test samples (Figure 3). We observe a mean binary agreement of 92.3% across all 40 attributes. As shown in the breakdown, distinct structural attributes such as *Eyeglasses*, *Hats*, and *Neckties* are reconstructed with near-perfect consistency ($> 97\%$). Conversely, the minor error variance is concentrated in subjective or ambiguous features (e.g., *High Cheekbones*, *Arched Eyebrows*), where the classifier’s own uncertainty is typically higher.

Attribute-Controlled Generation. We demonstrate the ability to control a specific attribute during generation without fixing the entire semantic vector. Here, we do not use a static target y . Instead, at each timestep t , we compute the semantic state of the current estimate: $y_{cur} = g(\hat{x}_{0|t})$. To enforce a target attribute n (e.g., "Eyeglasses"), we construct a dynamic target y_{target} by copying y_{cur} and modifying only the n -th index:

$$y_{target}[k] = \begin{cases} \mu_n + 2\sigma_n & \text{if } k = n \\ y_{cur}[k] & \text{otherwise} \end{cases} \quad (25)$$

where μ_n and σ_n denote the empirical mean and standard deviation of attribute n computed over the training set. We then apply the NLBP step using this y_{target} . Because y_{target} matches y_{cur} on all other dimensions, the update vector in the latent space is sparse (zero everywhere except at index n). This allows the diffusion model to freely hallucinate all other attributes, constrained only by the single trait we wish to enforce. Figure 4 shows that this dynamic guidance yields diverse, high-quality images that strictly adhere to the requested attribute. This capability naturally extends to compositional generation; as shown in Figure 5, we can simultaneously enforce multiple constraints (e.g., *Male +*



Figure 4. **Single Attribute Editing.** By dynamically enforcing a specific target index in the attribute vector (e.g., forcing the "Eyeglasses" logit to be high), we can generate diverse samples that strictly adhere to the condition while hallucinating the rest of the image freely. This demonstrates that the SPNN has successfully disentangled the specific semantic attribute from the null-space.

(*Eyeglasses + Smiling*), effectively guiding the diffusion process to the intersection of these semantic manifolds.

8.3. Ablation Study

To validate our framework, we compare against four ablated baselines: combining either a **Random** or **Minimum-Norm** auxiliary network r . To make sure the results are not a consequence of our proposed NLBP, We test them also on basic naive non-linear back-projection ($x' = x + g^\dagger(y) - g(g^\dagger(x))$). Fig 6 demonstrates that all ablated configurations result in catastrophic failure. Moreover, we applied the classifier to the generated failure images and none of them got logits close to the target. This confirms the algebra, showing that a change of metric is needed in order to adapt PInv and Back-Projection to the non-linear regime.

9. Discussion and Conclusion

Limitations Our framework has two primary limitations. First, the validity of the "Natural" PInv depends on the expressivity of the auxiliary network r . If r fails to capture the true null-space statistics, the pseudo-inverse remains algebraically correct ($gg^\dagger = I$) but may yield unrealistic pre-images. Second, we assume the forward operator g is surjective. In the general case where y lies outside the range of g , our definition is valid but G has more degrees of freedom. Defining a "natural" unique PInv remains an open question.

Future Work We envision three key extensions. First, we plan to apply SPNNs to complex degradations such as object detection, or optical distortions. Second, building on (Berman et al., 2025), we propose that surjectivity, rather

than strict invertibility, is sufficient for linearity, potentially enabling more efficient "Linearizers". Finally, we intend to replace Latent Diffusion Models' VAE encoders with SPNN blocks to solve cycle-consistency issues ($E(D(z)) \neq z$).

Conclusion In this work, we introduced the Natural Non-Linear Pseudo-Inverse via the concept of Affine Bijective Completion, offering a rigorous generalization of the linear Moore-Penrose inverse to deep networks. We realized this theory through the Surjective Pseudo-invertible Neural Network (SPNN), a dimension-reducing architecture that maintains an exact structural right-inverse. By combining SPNNs with our proposed Non-Linear Back-Projection (NLBP), we demonstrated a zero-shot restoration framework capable of inverting abstract semantic degradations. As deep learning increasingly replaces linear operators in scientific computing, we believe this principled formulation provides the essential mathematical bridge for analyzing and solving complex non-linear inverse problems.

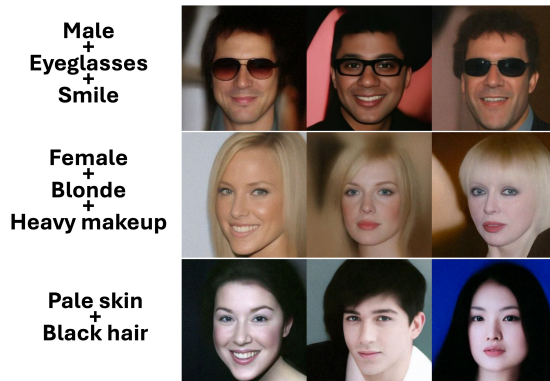


Figure 5. **Multi-Attribute Conditional Generation.** simultaneously enforcing constraints by fixing multiple bits in the target y .

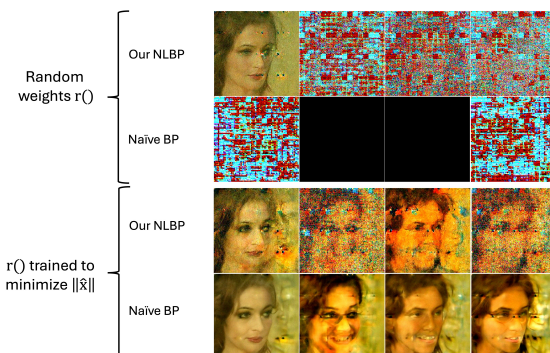


Figure 6. **Ablation Study.** We attempt to reconstruct the same four test samples from Figure 2 using ablated baselines (Random/Min-Norm $r \times$ Naïve/Gentle BP). In all configurations, the failure to learn the "Natural" manifold or apply gentle guidance causes the diffusion process to diverge into high-frequency noise.

Acknowledgments

A.S. is supported by the Chaya Career Advancement Chair.

Impact Statement

This paper presents a theoretical framework for defining and computing non-linear pseudo-inverses in deep neural networks. The primary goal of this work is to advance the mathematical foundations of inverse problems, offering rigorous tools for solving ill-posed challenges in scientific computing, medical imaging, and physics where non-linear measurement operators are prevalent.

We demonstrate the efficacy of our method through semantic restoration and attribute editing on facial images. We acknowledge that techniques for controlling generative models, such as the one proposed here, carry potential risks related to the creation of synthetic media and deepfakes. While our method is designed to enforce consistency with semantic constraints, the ability to modify attributes or reconstruct plausible identities from abstract descriptors could be misused for image manipulation.

Furthermore, our definition of the "Natural" pseudo-inverse relies on learning the geometry of the training data. Consequently, any biases present in the training dataset (e.g., correlations between specific demographic attributes and visual features) will be inherently captured by the Surjective Pseudo-invertible Neural Network (SPNN) and reflected in the reconstructed solutions. Researchers and practitioners applying this framework should be aware that the "canonical" solution provided by the model is only as neutral as the data distribution it was trained on.

References

- Berman, N., Hallak, A., and Shocher, A. Who said neural networks aren't linear? *arXiv preprint arXiv:2510.08570*, 2025.
- Chung, H., Sim, B., Ryu, D., and Ye, J. C. Improving diffusion models for inverse problems using manifold constraints. In *NeurIPS*, 2022.
- Chung, H., Kim, J., Mccann, M. T., Klasky, M. L., and Ye, J. C. Diffusion posterior sampling for general noisy inverse problems. In *ICLR*, 2023.
- Dinh, L., Krueger, D., and Bengio, Y. Nice: Non-linear independent components estimation. *arXiv preprint arXiv:1410.8516*, 2014.
- Dinh, L., Sohl-Dickstein, J., and Bengio, S. Density estimation using real nvp. In *ICLR*, 2017.
- Feistel, H. Cryptography and computer privacy. *Scientific American*, 228(5):15–23, 1973.
- Gofer, E. and Gilboa, G. Generalized inversion of nonlinear operators. *arXiv preprint arXiv:2111.10755*, 2023.
- Irani, M. and Peleg, S. Improving resolution by image registration. *CVGIP: Graphical Models and Image Processing*, 53(3):231–239, 1991.
- Kawar, B., Vaksman, G., and Elad, M. Snips: Solving noisy inverse problems stochastically. In *NeurIPS*, 2021.
- Kawar, B., Elad, M., Ermon, S., and Song, J. Denoising diffusion restoration models. In *NeurIPS*, 2022.
- Kingma, D. P. and Dhariwal, P. Glow: Generative flow with invertible 1x1 convolutions. In *NeurIPS*, 2018.
- Nielsen, D., Jaini, P., Hoogeboom, E., Winther, O., and Welling, M. Survae flows: Surjections to bridge the gap between vaes and flows. In *NeurIPS*, 2020.
- Penrose, R. A generalized inverse for matrices. *Proceedings of the Cambridge Philosophical Society*, 51(3):406–413, 1955.
- Trockman, A. and Kolter, J. Z. Orthogonalizing convolutional layers with the cayley transform. In *ICLR*, 2021.
- Wang, Y., Yu, J., and Zhang, J. Zero-shot image restoration using denoising diffusion null-space model. *arXiv preprint arXiv:2212.00490*, 2022.
- Wang, Y., Yu, J., and Zhang, J. Zero-shot image restoration using denoising diffusion null-space model. In *ICLR*, 2023.

A. Full quantitative results on attributes reconstruction

#	Attribute	Prob Diff	Agreement (%)
0	Blurry	0.0001	100
1	Eyeglasses	0.0046	100
2	Wearing Necktie	0.0065	100
3	Bald	0.0027	99
4	Gray Hair	0.0074	99
5	Sideburns	0.0086	98
6	Pale Skin	0.0144	98
7	Narrow Eyes	0.0157	98
8	Double Chin	0.0040	98
9	Mustache	0.0097	97
10	Wearing Hat	0.0158	97
11	Blond Hair	0.0304	97
12	Chubby	0.0106	96
13	Straight Hair	0.0058	95
14	Oval Face	0.0107	95
15	Goatee	0.0252	95
16	5 o Clock Shadow	0.0185	94
17	Receding Hairline	0.0129	94
18	Wearing Necklace	0.0157	94
19	Heavy Makeup	0.0443	93
20	Wearing Lipstick	0.0463	93
21	Male	0.0499	93
22	Bags Under Eyes	0.0127	92
23	Black Hair	0.0247	92
24	Brown Hair	0.0292	92
25	Bangs	0.0357	92
26	No Beard	0.0501	91
27	Young	0.0340	89
28	Wavy Hair	0.0229	89
29	Smiling	0.0572	88
30	Big Lips	0.0084	87
31	Bushy Eyebrows	0.0249	87
32	High Cheekbones	0.0560	87
33	Pointy Nose	0.0208	86
34	Big Nose	0.0259	86
35	Rosy Cheeks	0.0566	85
36	Attractive	0.0292	83
37	Wearing Earrings	0.0454	82
38	Arched Eyebrows	0.0534	81
39	Mouth Slightly Open	0.0989	80

B. Implementation details

B.1. Back-Projection Guidance Scheduling.

Semantic reconstruction. For reconstruction tasks, BP guidance is applied throughout the entire reverse diffusion process, covering all timesteps ($t \in [1000, 0]$), in order to preserve the global semantic structure established early in generation.

Single-attribute editing. For single-attribute manipulation, BP guidance is restricted to the later stages of the reverse process, with guidance enabled only for ($t \in [500, 0]$). At earlier timesteps ($t > 500$), the BP step size is set to zero, allowing the diffusion prior to establish global structure before fine-grained attribute control is introduced.

Multi-attribute editing. For multi-attribute editing, we extend the guidance window to $(t \in [800, 0])$ to account for the increased semantic coupling between attributes. As in the single-attribute case, BP guidance is disabled at earlier timesteps by setting the step size to zero.

B.2. Covariance Adjustment.

Naive modification of a single attribute (e.g., forcing "Beard" to 1) can create an adversarial target vector if correlated attributes (e.g., "Male") are not adjusted essentially. To maintain a plausible target y_{target} , we utilize the empirical covariance matrix Σ of the training attributes. When modifying index n by an amount Δy_n , we adjust all other indices $j \neq n$ according to their linear correlation:

$$\Delta y_j = \frac{\Sigma_{jn}}{\Sigma_{nn}} \Delta y_n. \tag{26}$$

This ensures that the target vector y_{target} lies on the natural manifold of attribute correlations, preventing the generation of out-of-distribution artifacts.

In practice, we consider two complementary strategies for modifying attribute values: the covariance-based adjustment described above, which is used for highly correlated attributes, and a sparse single-attribute modification strategy (Eq. 25), which is applied to weakly correlated attributes such as *Eyeglasses*.

B.3. Architecture & Hyper-parameters.

Table 1. SPNN Architecture and Training Configuration

Category	Setting
Model Architecture	
Input resolution	256 × 256 RGB
Number of SPNN blocks	5
Orthogonal mixing	Cayley 1 × 1 convolutions
Latent partitioning	Channel-wise
Activation (scale)	tanh(·) × 2.0, then exp
Number of attributes	40 (CelebA-HQ)
Training Setup	
Dataset	CelebA-HQ
Batch size	256
Optimizer	Adam
Learning rate	2 × 10 ⁻⁴
Adam (β_1, β_2)	(0.9, 0.999)
Epochs	15
Gradient clipping	1.0
Warmup iterations	200
Precision	FP32 (float16=False)
Random seed	556
Loss Weights	
λ_{task}	1.0
λ_{surj}	40.0
λ_{stab}	40.0
$\lambda_{natural}$	0.3
λ_{r_surj}	1.0
λ_{r_stab}	1.0
r -optimization epochs	50
r -optimization learning rate	1 × 10 ⁻⁴
r -optimization batch size	256

Table 2. Diffusion Model and Sampling Configuration

Category	Setting
Data Configuration	
Dataset	CelebA-HQ
Image resolution	256×256
Channels	3 (RGB)
Logit transform	Disabled
Uniform dequantization	Disabled
Gaussian dequantization	Disabled
Random horizontal flip	Enabled
Rescaled input	Enabled
Out-of-distribution data	Disabled
Data loader workers	32
Model Architecture	
Model type	Simple U-Net
Input / output channels	3 / 3
Base channel width	128
Channel multipliers	[1, 1, 2, 2, 4, 4]
Residual blocks per level	2
Self-attention resolutions	16
Dropout	0.0
Variance type	FixedSmall
EMA	Enabled
EMA decay rate	0.999
Resampling with convolution	Enabled
Diffusion Process	
Noise schedule	Linear
β_{start}	1×10^{-4}
β_{end}	2×10^{-2}
Number of diffusion steps	1000
Sampling & Time-Travel Parameters	
Sampling batch size	1
Sampling horizon (T_{sampling})	100
Travel length	1
Travel repeat (reconstruction)	1
Travel repeat (attribute editing)	2